Study of the phase diagram of dense two-color QCD within lattice simulation

V. V. Braguta,[1,2,3,4,*] E.-M. Ilgenfritz,[5,†] A. Yu. Kotov,[2,6,‡] A. V. Molochkov,[3,§] and A. A. Nikolaev[3,2,‖]

[1]*Institute for High Energy Physics NRC "Kurchatov Institute", Protvino 142281, Russia*
[2]*Institute for Theoretical and Experimental Physics NRC "Kurchatov Institute", Moscow 117218, Russia*
[3]*School of Biomedicine, Far Eastern Federal University, Sukhanova 8, Vladivostok 690950, Russia*
[4]*Moscow Institute of Physics and Technology, Institutskii per. 9, Dolgoprudny, Moscow Region 141700, Russia*
[5]*Joint Institute for Nuclear Research, BLTP, Dubna 141980, Russia*
[6]*National Research Nuclear University MEPhI (Moscow Engineering Physics Institute), Kashirskoe Highway, 31, Moscow 115409, Russia*

(Received 6 July 2016; published 15 December 2016)

In this paper, we carry out a low-temperature scan of the phase diagram of dense two-color QCD with $N_f = 2$ quarks. The study is conducted using lattice simulation with rooted staggered quarks. At small chemical potential, we observe the hadronic phase, where the theory is in a confining state, chiral symmetry is broken, the baryon density is zero, and there is no diquark condensate. At the critical point $\mu = m_\pi/2$, we observe the expected second-order transition to Bose-Einstein condensation of scalar diquarks. In this phase, the system is still in confinement in conjunction with nonzero baryon density, but the chiral symmetry is restored in the chiral limit. We have also found that in the first two phases the system is well described by chiral perturbation theory. For larger values of the chemical potential, the system turns into another phase, where the relevant degrees of freedom are fermions residing inside the Fermi sphere, and the diquark condensation takes place on the Fermi surface. In this phase, the system is still in confinement, chiral symmetry is restored, and the system is very similar to the quarkyonic state predicted by SU(N_c) theory at large N_c.

DOI: 10.1103/PhysRevD.94.114510

I. INTRODUCTION

The phase diagram of QCD is of high importance for several fields of observational physics like cosmology and astrophysics. One field of experimental physics, located between nuclear physics and high-energy physics, is the study of hadronic matter created by relativistic heavy ion collisions. Such experiments are addressing the structure of the phase diagram, although the understanding and modeling of an actual collision requires much more than the knowledge of the equilibrium phase diagram. However, equilibrium observables like the equation of state and transport coefficients are highly needed to be used in hydrodynamical approaches which serve to probe various scenarios.

The region of high temperature and vanishing baryonic density of the QCD phase diagram is well explored at the LHC and Relativistic Heavy Ion Collider (RHIC). The theoretical study of this part of the phase diagram can be carried out with lattice gauge theory (LGT), based on the first principles of QCD. Today, this approach has reached a high level of maturity, and the results obtained within LGT for small μ/T are in good agreement with experiments [1,2].

In the 2010s, a "low-energy frontier" of heavy ion physics has opened (with the beam energy scan program at the RHIC) focussing on the region of high baryonic density and lower temperatures. The new experimental facilities presently under construction, Facility for Antiproton and Ion Research (FAIR) and Nuclotron-based Ion Collider fAcility (NICA), hosting the future experiments Compressed Baryonic Matter (CBM), Baryonic Matter at Nuclotron (BM&N), and Multi Purpose Detector (MPD), respectively, will be suitable for this region of the phase diagram. This situation is urging theorists to study QCD with large chemical potential.

Unfortunately, lattice simulation of QCD cannot be applied today to arbitrary chemical potential because of the sign problem [3]. The origin of the sign problem is that the fermion determinant becomes complex valued, and direct simulation by importance sampling of gauge field configurations is not possible. In the absence of straightforward results from LGT, one applies different approaches to study the (T, μ) phase diagram: for instance, mean field approaches [4], the method of Dyson-Schwinger equations [5], the large-N_c approach [6,7], perturbative QCD coupled to HRG models [8], exploring the phase diagram of QCD with isospin chemical potential [9–13], and others. Although the results obtained within these approaches are very interesting, they may still be rather schematic and require confirmation.

An alternative to lattice simulation of SU(3) QCD with $\mu \neq 0$ is the simulation of SU(2) QCD (also called QC_2D).

*braguta@itep.ru
†ilgenfri@theor.jinr.ru
‡kotov@itep.ru
§molochkov.av@dvfu.ru
‖nikolaev.aa@dvfu.ru

Introduction of a chemical potential to the latter theory does not lead to a sign problem, so one can apply the standard lattice approach to study this theory. Although a two-color world differs from the tree-color world, a lattice study of QC_2D with chemical potential can provide us with important information about the properties of QCD with nonzero baryon density. In particular, we believe that some physical properties of the regions of the phase diagram where relevant degrees of freedom are quarks and gluons are similar for the SU(2) and SU(3) theories [7]. As an example, one could mention the equation of state, some properties of the gluon propagator (for instance, Debye screening), generation of the fermion mass gap, etc. In addition, one can use SU(2) QCD to study how nonzero density influences different observables and phenomena. We would like also to note that the QC_2D phase diagram has a rich structure, and it is interesting to study on its own.

The properties of QC_2D were studied theoretically within the following approaches: chiral perturbation theory (ChPT) [14–18], the NJL model [19–22], the functional renormalization group [23–26], and the random matrix theory [27–29]. Principally, these studies have revealed the following phase structure of low-temperature QC_2D with three subsequent phases: 1) $0 < \mu < \mu^c$ (hadronic phase), 2) $\mu^c < \mu < \mu^d$ ("baryon onset" with a superfluid condensate due to Bose-Einstein condensation [BEC]), and 3) $\mu^d < \mu$ (the phase with diquark condensation due to the Bardeen-Cooper-Schrieffer mechanism [BCS] [30]).

The first lattice study of QC_2D with chemical potential and Wilson fermions was performed by A. Nakamura in Ref. [31]. Further lattice investigation of dense two-color QCD was continued by J. Kogut and collaborators [32] using staggered quarks. The staggered Dirac operator without rooting describes $N_f = 4$ flavors. Making the whole fermion matrix Hermitian positive definite by doubling the number of flavors has lead to the eight-flavor theory investigated in the pioneering paper [32]. Following this work, introduction of the rooting trick for the staggered fermion determinant has allowed us to investigate the case of $N_f = 4$ flavors in more detail [33–35]. The main activity in two-color QCD was later continued by the Swansea group (S. Hands and collaborators), mainly for the two-flavor theory, with each flavor described by one species of Wilson fermions [36–39].

In this paper, we are going to study the QC_2D phase diagram with $N_f = 2$ flavors going back to the lattice simulation of staggered fermions using the rooting procedure. The advantage of the staggered fermion formulation is the approximate residual chiral symmetry of the Dirac operator [40]. Therefore, we have chosen this formulation to complement the Swansea studies by an alternative study of the two flavors case. In our first paper [41], we calculated the Polyakov loop and the chiral condensate as functions of temperature for different values of the chemical potential μ [42]. In the present paper, we are going to carry out a μ scan at low temperature of the QC_2D phase diagram.

The paper is organized as follows. In Sec. II, we specify details of the lattice setup to be used: action, the way of the diquark source introduction, and details of the simulation. In Sec. III, we present the numerical results of this study. The last section is devoted to the discussion of the results and to some conclusions to be drawn.

II. LATTICE SET-UP

A. Partition function

In our simulations, we used the Wilson action for the SU(2) gauge fields

$$S_G = \beta \sum_x \sum_{\mu<\nu=1}^{4} \left(1 - \frac{1}{2}\mathrm{Tr} U_{x,\mu\nu}\right). \tag{1}$$

For the fermionic degrees of freedom, we used staggered fermions with an action of the form

$$S_F = \sum_{x,y} \bar{\psi}_x M(\mu, m)_{x,y} \psi_y + \frac{\lambda}{2} \sum_x (\psi_x^T \tau_2 \psi_x + \bar{\psi}_x \tau_2 \bar{\psi}_x^T), \tag{2}$$

$$M_{xy} = ma\delta_{xy} + \frac{1}{2}\sum_{\mu=1}^{4} \eta_\mu(x)[U_{x,\mu}\delta_{x+\hat{\mu},y} e^{\mu a \delta_{\mu,4}} - U^\dagger_{x-\hat{\mu},\mu}\delta_{x-\hat{\mu},y} e^{-\mu a\delta_{\mu,4}}], \tag{3}$$

where $\bar{\psi}$, ψ are staggered fermion fields, a is the lattice spacing, m is the bare quark mass, and $\eta_\mu(x)$ are the standard staggered phase factors: $\eta_1(x) = 1$, $\eta_\mu(x) = (-1)^{x_1+\cdots+x_{\mu-1}}$, $\mu = 2, 3, 4$. The chemical potential μ is introduced into Eq. (3) through the multiplication of the links along and opposite to the temporal direction by factors $e^{\pm\mu a}$, respectively. This way of introducing the chemical potential makes it possible to avoid additional divergences and to reproduce well-known continuum results [43].

In addition to the standard staggered fermion action, we add a diquark source term [32] to Eq. (2). The diquark source term explicitly violates $U_V(1)$ and allows us to observe diquark condensation even on finite lattices, because this term effectively chooses one vacuum from the family of $U_V(1)$-symmetric vacuums. The results presented in this paper are obtained as follows: we carry out simulations at small but nonzero parameter $\lambda \ll ma$ and then extrapolate obtained data to $\lambda \to 0$. Notice that, similar to the diquark source term, an additional pion term was introduced to the fermion action during the studies of the QCD phase diagram with isospin chemical potential [10,11,13].

Integrating out the fermion fields, the partition function for the theory with the action $S = S_G + S_F$ can be written in the form

$$Z = \int DUe^{-S_G} \cdot Pf \begin{pmatrix} \lambda\tau_2 & M \\ -M^T & \lambda\tau_2 \end{pmatrix} = \int DUe^{-S_G} \cdot (\det(M^\dagger M + \lambda^2))^{\frac{1}{2}}, \quad (4)$$

which corresponds to $N_f = 4$ dynamical fermions in the continuum limit. Note that the Pfaffian Pf is strictly positive, such that one can use hybrid Monte Carlo methods to study this system. The lattice study of the theory with partition function (4) was carried out in papers [33–35]. In the present paper, we are going to study the theory with the partition function

$$Z = \int DUe^{-S_G} \cdot (\det(M^\dagger M + \lambda^2))^{\frac{1}{4}}, \quad (5)$$

which corresponds to $N_f = 2$ dynamical fermions in the continuum limit. Notice that the diquark source term lifts the lowest eigenvalues of the matrix in determinant (5) and thus lowers the cost of numerical simulations.

It is known that the symmetries of the staggered fermion action are different from those of two-color QCD with fundamental quarks [32]. In particular, the symmetry breaking pattern of QC_2D with fundamental quarks is $SU(2N_f) \to Sp(2N_f)$, whereas for staggered quarks, it is $SU(2N_f) \to O(2N_f)$. However, it is easy to show that the diquark source term in the continuum limit can be written as

$$\frac{\lambda}{2}\sum_x (\psi_x^T\tau_2\psi_x + \bar\psi_x\tau_2\bar\psi_x^T)|_{a\to 0} = \frac{\lambda}{2}\int d^4x (q_i^T C\gamma_5\tau_2 q_j + \bar q_i C\gamma_5\tau_2\bar q_j^T) \times \begin{pmatrix} \boldsymbol{\sigma_2} & 0 \\ 0 & \boldsymbol{\sigma_2} \end{pmatrix}_{ij}.$$

So in the naive continuum limit for the diquark source term, we have two copies of fundamental fermions. Thus, one can expect that the partition function (5) after the rooting procedure corresponds to QC_2D with $N_f = 2$ fundamental fermions. Moreover, for sufficiently small lattice spacing a, the β function of the theory (5) corresponds to the β function of QC_2D with two fundamental flavors (see below). For these reasons, we believe that the partition function (5) in the continuum limit describes QC_2D with $N_f = 2$ fundamental fermions.

B. Observables

In our simulations, we measured the following observables:

(i) the Polyakov loop:

$$\langle L\rangle = \frac{1}{N_s^3}\sum_{x_1,x_2,x_3=0}^{N_s-1}\frac{1}{2}\left\langle \mathrm{Tr}\prod_{x_4=0}^{N_\tau-1} U_{x,4}\right\rangle; \quad (6)$$

(ii) the timelike Wilson loop around a rectangular contour $C = R \times T$:

$$W(R,T) = \left\langle \mathrm{Tr}\left[\prod_C U_{x,\mu}\right]\right\rangle; \quad (7)$$

(iii) the chiral condensate:

$$a^3\langle\bar q q\rangle = a^3\langle\bar q_{i\alpha}q_{i\alpha}\rangle = -\frac{1}{N_s^3N_\tau}\frac{\partial(lnZ)}{\partial(ma)}; \quad (8)$$

(iv) the baryon density:

$$a^3 n_B = a^3\frac{1}{2}\langle\bar q_{i\alpha}\gamma_0 q_{i\alpha}\rangle = \frac{1}{2}\frac{1}{N_s^3N_\tau}\frac{\partial(lnZ)}{\partial(\mu a)}; \quad (9)$$

(v) the diquark condensate:

$$a^3\langle qq\rangle = -\frac{1}{N_s^3N_\tau}\frac{\partial(lnZ)}{\partial\lambda} = a^3\langle q_{i\alpha}^T\hat C\gamma_5(\tau_2)_{ij}(\sigma_2)_{\alpha\beta}q_{j\beta}\rangle. \quad (10)$$

In formulas (8)–(10), the fields $\bar q, q$ are quark fields in the continuum theory, $\hat C$ is the matrix of charge conjugation, and τ_2 and σ_2 are flavor and color Pauli matrices, respectively. The quark fields have Dirac (not shown for the sake of brevity), color (α, β), and flavor indices (i, j). Summation over repeated indices is tacitly understood. Notice that in addition to the quark contribution there is a similar antiquark contribution to Eq. (10), which is not shown. This is because we work with positive chemical potential and in this region the antiquark contribution to the equation (10) is exponentially suppressed. In numerical calculations of the diquark condensate, we have taken into account both quark and antiquark contributions.

The Polyakov and Wilson loops are meant to be sensitive to an eventual confinement/deconfinement phase transition. The chiral condensate is sensitive to breaking/restoration of the chiral symmetry. The diquark condensate is an order parameter for the transition to a phase, where scalar diquarks are condensed.

C. Details of the simulation

To study the phase diagram of QC_2D with $N_f = 2$ flavors we used a $16^3 \times 32$ lattice, simulating with $\beta = 2.15$ and $ma = 0.005$, which corresponds to a fixed temperature $T \approx 55$ MeV, lattice spacing $a = 0.112(1)$ fm, pion mass $M_\pi = 378(4)$ MeV, and $m_\pi L_s \approx 3.4$ (see Sec. II D). The simulation was carried out for a set of values of the chemical potential μ spanning the region $\mu \in [0; 1759]$ MeV ($\mu a \in [0.0; 1.0]$). For each value of μ in the region $\mu \in [0; 1055]$ MeV ($\mu a \in [0.0; 0.6]$), we carried out the simulation at three values of the diquark source $\lambda = 0.001$, 0.00075, and 0.0005. The measured data were then extrapolated to $\lambda = 0$. In the vicinity of the phase transition from the hadronic phase to the BEC phase $\mu = 176$, 211, 246 MeV ($\mu a = 0.1$, 0.12, 0.14,

respectively), we carried out simulations at five values of the diquark source: $\lambda = 0.001$, 0.000875, 0.00075, 0.000625, and 0.0005. Simulations with higher μ are more computationally demanding, and thus for $\mu > 1055$ MeV ($\mu a > 0.6$), only one value of the diquark source, $\lambda = 0.0005$, was used.

In the simulations, we used the RHMC algorithm [44,45]. The fourth root in the action evaluation was approximated with the accuracy $\sim O(10^{-15})$. For each pair of μ and λ, we generated 1000–1500 MD trajectories after thermalization and performed measurements of the Polyakov loop (6) at each trajectory and of the fermionic observables (8)–(10) at each tenth trajectory. We employed the stochastic estimation technique with Gaussian random sources to calculate fermionic traces and used 100–250 Gaussian random vectors per trace.

It is worth mentioning that we carried out a check of our simulation program through the comparison of our results with the QC_2D results existing in the literature. In particular, we compared with the results of simulation of staggered fermions without rooting and chemical potential [46], of staggered $N_f = 2$ flavors and with $\mu = 0$ [47], and of staggered $N_f = 4$ flavors with nonzero chemical potential and nonzero diquark source [35]. For all these cases, we found good agreement.

D. Scale setting and pion mass

First, we performed additional measurements at zero values of the baryon chemical potential μ in order to calculate the β function and the pion mass, because the behavior of the β function provides a natural check for the correct continuum limit. In these simulations, we used a lattice with the size $16^3 \times 32$ as well. To fix the physical scale, we extracted the heavy quark potential from smeared Wilson loops (1 hypercubic smearing [48] step for temporal links was employed, followed by 20 Ape Collaboration smearing [49] steps for spatial links; the details are described in Ref. [50]). From this potential, we extracted the Sommer scale parameter r_0. Assuming that it is equal to the Sommer scale parameter in real QCD, $r_0 = 0.468(4)$ fm in physical units [51], we determined the lattice spacing.

To carry out the scale setting, we fixed the quark mass $ma = 0.005$ and the diquark source $\lambda = 0.0005$ and varied $\beta \in [2.1; 2.25]$. 4000 MD trajectories were generated for each value of β, and measurements were performed at every tenth trajectory. The results of the simulation are presented in Table I and in Fig. 1.

TABLE I. The lattice spacing a and the pion mass m_π for various values of the inverse coupling β for the bare quark mass $ma = 0.005$ and $\lambda = 0.0005$.

β	a, fm	M_π, MeV
2.1	0.129(1)	329(3)
2.15	0.112(1)	377(4)
2.2	0.095(2)	493(8)
2.25	0.082(1)	561(9)

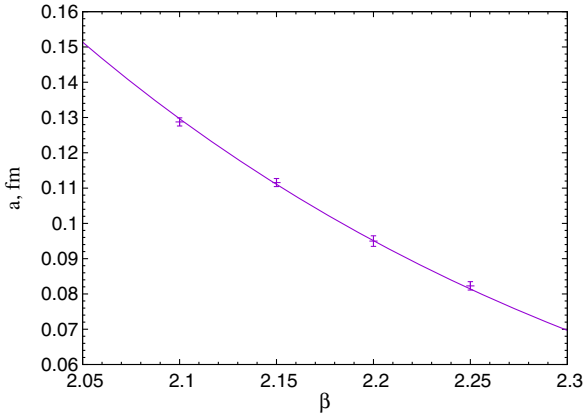

FIG. 1. The dependence of the lattice spacing on the inverse coupling $\beta = 4/g^2$.

We found that for all considered values of β the dependence of the lattice spacing a can be reasonably fitted with the two-loop formula with $N_c = 2$ and $N_f = 2$,

$$a(\beta) = \frac{1}{\Lambda_L}\left(\frac{4\beta_0}{\beta}\right)^{-\frac{\beta_1}{2\beta_0^2}} \exp\left(\frac{-\beta}{8\beta_0}\right),$$
$$\beta_0 = \frac{3}{8\pi^2}, \qquad \beta_1 = \frac{29}{256\pi^4}, \tag{11}$$

with $\chi^2/\mathrm{dof} = 0.47$ and $\Lambda_L = 0.0222(1)$ fm^{-1} [52]. Good agreement between our data and the formula (11) for the β function provides an argument that the partition function (5) in the continuum limit describes QC_2D with $N_f = 2$ fundamental fermions.

To measure the pion masses, we calculated the pion propagators $C_\pi(t, \vec{q} = 0)$ for the same parameter sets, which were used for the scale setting. From the fit of the pion propagators with the usual cosh form, $C_\pi(t, \vec{q} = 0) = C\cosh(-m_\pi(t - T/2))$, we extracted the pion masses, which are also presented in Table I in physical units. We also checked that the results for Wilson loops and pion masses are practically independent of the value of the diquark source. For instance, at $\beta = 2.15$ for the $\lambda = 0.0$, the pion mass is $m_\pi = 378(4)$; for the $\lambda = 0.0005$, the pion mass is $m_\pi = 377(4)$ MeV, and for the $\lambda = 0.001$, the pion mass is $m_\pi = 382(4)$ MeV. We would like to note that the pion mass in our study is smaller compared to previous studies [33–39].

III. NUMERICAL RESULTS

A. Diquark condensate

In this section, we are going to study the diquark condensate. It was noted above that in the region $\mu \in [0.0; 1055]$ MeV ($\mu a \in [0.0; 0.6]$) the condensate is calculated for three values of the diquark source: $\lambda = 0.0005$,

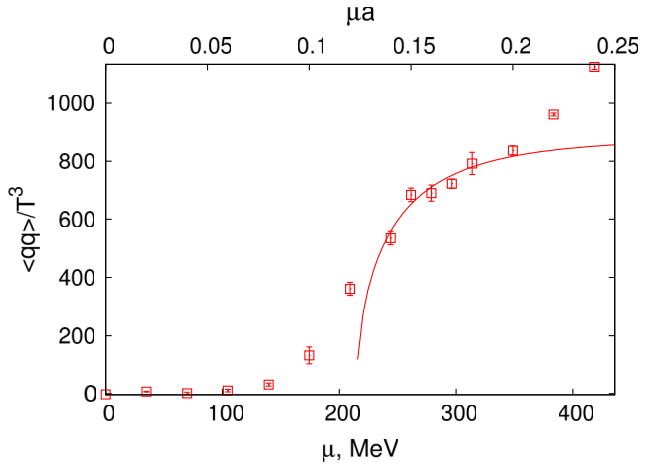

FIG. 2. The diquark condensate $\langle qq\rangle/T^3$ as a function of μ. The chemical potential is expressed in physical units (lower scale) and in lattice units (upper scale). The data are fitted by function (12).

0.00075, and 0.001. To extrapolate our results to $\lambda \to 0$, we used a linear fit [53] of the data for all values of the chemical potential under investigation. The linear fit turned out to be good ($\chi^2/\mathrm{dof} \sim 1$) in the region $\mu \leq 141$ MeV ($\mu a \leq 0.08$) and $\mu \geq 263$ MeV ($\mu a \geq 0.15$). For the values $\mu a = 176$, 211, and 246 MeV ($\mu a = 0.1$, 0.12, 0.14, respectively), a linear fit does not describe the data well. We believe that this fact can be explained by the closeness of these μ values to the critical chemical potential μ^c, where the system undergoes the phase transition from the hadronic phase to the phase with $\langle qq\rangle \neq 0$.

In Fig. 2, we plot the diquark condensate $\langle qq\rangle$ (obtained by linear extrapolation to $\lambda = 0$) as a function of μ in the region $\mu \in [0.0; 440]$ MeV ($\mu a \in [0.0; 0.25]$). It may be seen that for $\mu \leq 141$ MeV ($\mu a \leq 0.08$) the diquark condensate $\langle qq\rangle$ is compatible with zero. However, for $\mu \geq 176$ MeV ($\mu a \geq 0.1$), the diquark condensate starts to deviate from zero. If we are sufficiently far from the position of the phase transition, one can try to use ChPT to describe the data [14–17]. In particular, ChPT predicts that the transition from the hadronic phase to the phase with $\langle qq\rangle \neq 0$ takes place at $\mu^c = m_\pi/2$, and the behavior of the diquark condensate above the transition would be given by the formula

$$\langle qq\rangle = \langle \bar{q}q\rangle_0 \sqrt{1 - \left(\frac{\mu^c}{\mu}\right)^4}, \qquad (12)$$

where $\langle \bar{q}q\rangle_0$ is the chiral condensate at zero chemical potential. If one uses formula (12) to fit our data in the region $\mu \in [263; 352]$ MeV ($\mu a \in [0.15; 0.20]$), one gets $\mu^c = 215(10)$ MeV ($a\mu^c = 0.122(6)$) with $\chi^2/\mathrm{dof} = 2.5$. We plot the function (12) in Fig. 2.

One can try to fit the data by another function. To build it, we recall that in the ChPT the diquark condensate can be determined from the equation $\langle qq\rangle = \sqrt{\langle \bar{q}q\rangle_0^2 - \langle \bar{q}q\rangle^2}$. In the ChPT for the $\mu > \mu^c$, the chiral condensate $\langle \bar{q}q\rangle$ drops with the chemical potential as $\sim 1/\mu^2$, and thus one gets (12). However, our data show (see below) that the chiral condensate drops more slowly: $\langle \bar{q}q\rangle \sim 1/\mu^\alpha$ with $\alpha = 0.78(2)$. Thus, it is reasonable to fit the data by the formula

$$\langle qq\rangle = \langle \bar{q}q\rangle_0 \sqrt{1 - \left(\frac{\mu^c}{\mu}\right)^{2\alpha}}, \qquad (13)$$

with the power α mentioned above. The fit of the data by formula (13) in the region $\mu \in [263; 352]$ MeV ($\mu \in [0.15, 0.20]$) gives $\mu^c = 193(10)$ MeV [$a\mu^c = 0.110(6)$] with $\chi^2/\mathrm{dof} = 1.4$.

From these examples, one sees that the position of the critical point determined from the fitting procedure strongly depends on the fitting function. Nevertheless, one can state that the results for μ^c are in reasonable agreement with ChPT.

It is interesting to study the limit $\lambda \to 0$ of our data in the vicinity of the phase transition at $\mu = 176$, 210 and 246 MeV. For these values of the chemical potential, the diquark condensate was measured at five points: $\lambda = 0.0005$, 0.000625, 0.00075, 0.000825, and 0.001. From ChPT, we know that at the critical chemical potential $\mu = \mu^c$ the behavior of the diquark condensate should be like $\langle qq\rangle \sim \lambda^{1/3}$. Thus, it is reasonable to fit the data in the vicinity of the phase transition by the function $\langle qq\rangle = A + B\lambda^{1/3}$. The results of the fit are shown in Fig. 3. For all three values of the chemical potential, the fit is good: $\chi^2/\mathrm{dof} \sim 1$. We found that for the smallest chemical potential value $\mu = 176$ MeV ($\mu a = 0.1$) the extrapolated value of the diquark condensate is negative: $\langle qq\rangle|_{\lambda\to 0} = -0.012(2)$. A negative value of the condensate can be attributed to the fact that the value $\mu = 176$ MeV is rather far from the critical point. For the next value $\mu = 211$ MeV ($\mu a = 0.12$), the condensate is compatible with zero: $\langle qq\rangle|_{\lambda\to 0} = -0.0021(12)$. Finally, for the largest

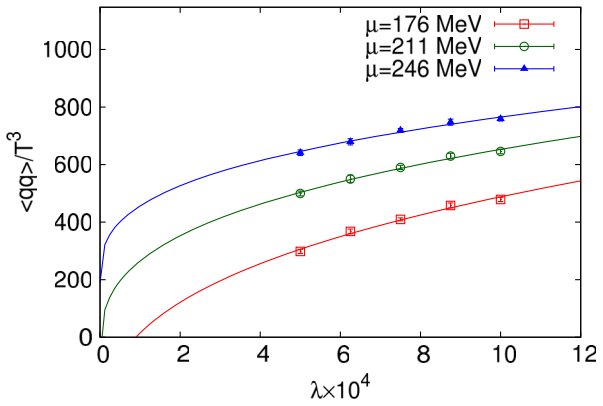

FIG. 3. The diquark condensate $\langle qq\rangle/T^3$ as a function of λ in the vicinity of the phase transition.

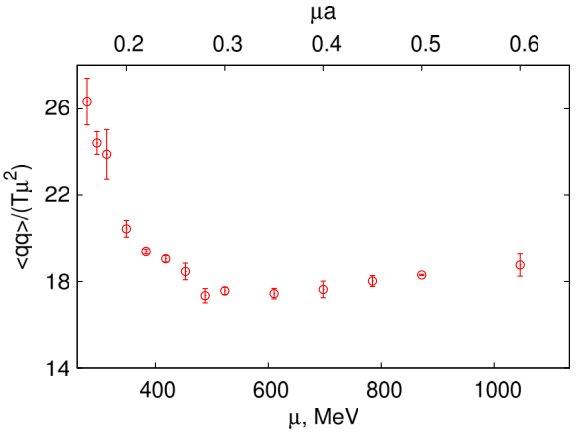

FIG. 4. The ratio $\langle qq\rangle/(T\mu^2)$ as a function of μ. The chemical potential is expressed in physical units (lower scale) and in lattice units (upper scale).

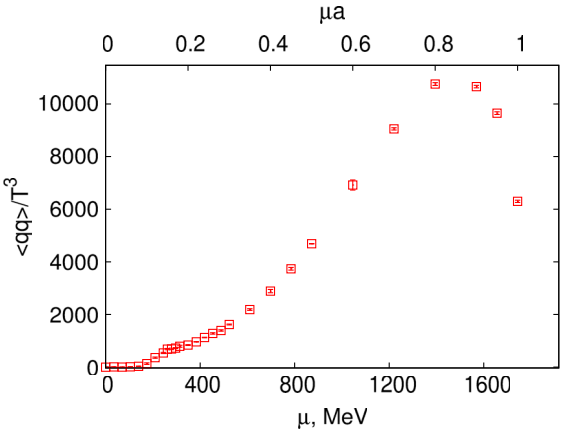

FIG. 5. The diquark condensate $\langle qq\rangle/T^3$ as a function of μ. The chemical potential is expressed in physical units (lower scale) and in lattice units (upper scale).

value $\mu = 246$ MeV ($\mu a = 0.14$), the condensate is greater than zero: $\langle qq\rangle|_{\lambda\to 0} = 0.0058(14)$. These results indicate that $\mu = 211$ MeV ($\mu a \simeq 0.12$) is closer to the critical point than $\mu = 176$ MeV ($\mu a = 0.1$) and $\mu = 246$ MeV ($\mu a = 0.14$), which agrees within the uncertainty with the value of the critical point obtained above.

To summarize, in the region $\mu < \mu^c$, the system is in the hadronic phase with zero diquark condensate. In the region $\mu > \mu_c$, the system is in the BEC phase with nonzero diquark condensate. In the region $\mu \in [0.0; 352]$ MeV ($\mu a \in [0.0; 0.20]$), our results for the diquark condensate are in good agreement with ChPT predictions. From Fig. 2, one sees that in the region $\mu > 352$ MeV ($\mu a > 0.2$) the data start to deviate from ChPT description.

Let us consider the region of larger chemical potential $\mu > 352$ MeV ($\mu a > 0.2$). To understand what happens in this region, we plot in Fig. 4 the linearly extrapolated diquark condensate, divided by $T\mu^2$, as a function of μ. As is visible from this plot, in the region $\mu \in [528; 1055]$ MeV ($\mu a \in [0.3; 0.6]$), there is a plateau; i.e., the value of the diquark condensate is proportional to the surface of a sphere with the radius μ: $\langle qq\rangle \sim \mu^2$. This is a characteristic property of the BCS theory, where the condensate appears on the Fermi surface and where it is proportional to the density of states on this surface. Thus, we conclude that for $\mu > 528$ MeV ($\mu a > 0.3$) the system reveals properties of the BCS phase and that the transition from the BEC to the BCS phase is smooth.

It is worth noting that in Ref. [35] $N_f = 4$ theory was simulated on the 16^4 lattice at $\beta = 1.85$ with $ma = 0.05$ and the BCS phase has not been observed. According to Ref. [46], the lattice spacing for this set of parameters is larger than lattice spacing in our simulations. In our study of the critical chemical potential, $\mu^c a \simeq 0.12$, whereas in Ref. [35], it was found that $\mu^c a \simeq 0.29$. From the relation $\mu^c = m_\pi/2$, one might conclude that in Ref. [35] the pion is more than two times heavier than in our simulations. This remarkable physical difference may be the reason why in the previous studies with $N_f = 4$ the BCS phase was not realized.

In the region $\mu > 1055$ MeV ($\mu a > 0.6$), the simulations become very computationally demanding. At the same time, in this region, the value of the diquark condensate becomes less sensitive to the value of the source λ, compared to the BEC phase. We believe that this might be related to the fact that the larger the μ, the larger the fermion mass gap, which plays a role of the regulator of the fermion determinant. For this reason, for $\mu > 1055$ MeV ($\mu a > 0.6$), we used $\langle qq\rangle|_{\lambda=0.0005}$ as the estimate of the value of the condensate at $\lambda = 0$. In Fig. 5, we plot the diquark condensate $\langle qq\rangle$ as a function of μ throughout the whole region under study. In the region $\mu > 1055$ MeV ($a\mu > 0.6$), the condensate starts to deviate from the BCS behavior, and after $\mu > 1410$ MeV ($a\mu > 0.8$), the condensate decreases. Such a descent of the diquark condensate $\langle qq\rangle$ in the region $\mu a \sim 1$ was already observed in Refs. [34,35]. This behavior might be connected with a saturation effect and therefore can be considered as a lattice artifact.

B. Chiral condensate

Next, let us consider the chiral condensate $\langle \bar{q}q\rangle$. In Fig. 6, we plot the chiral condensate as a function of μ in the region $\mu \in [0.0; 440]$ MeV ($\mu a \in [0.0; 0.25]$) for the following three values of the diquark source: $\lambda = 0.001$, 0.00075, and 0.0005. From Fig. 6, it is obvious that the dependence of the chiral condensate on the source λ is very weak. Except for a few fluctuations, the values of the chiral condensate $\langle \bar{q}q\rangle$, calculated at different values of λ, are equal to each other within the uncertainties. The next observation is that up to $\mu < 176$ MeV ($\mu a < 0.1$) the chiral condensate does not depend on the chemical potential. In the region $\mu > 176$ MeV, where the system is in the vicinity of the transition to the BEC phase, the chiral

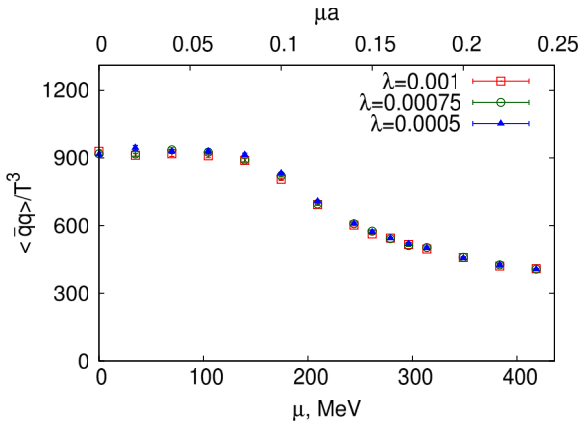

FIG. 6. The chiral condensate $\langle\bar{q}q\rangle/T^3$ as a function of μa for the values $\lambda = 0.001$, 0.00075, and 0.0005 of the diquark source. The chemical potential is expressed in physical units (lower scale) and in lattice units (upper scale).

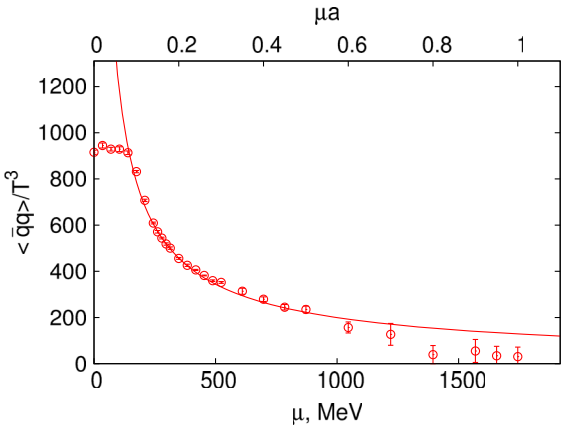

FIG. 8. The chiral condensate $\langle\bar{q}q\rangle/T^3$ as a function of μ. The chemical potential is expressed in physical units (lower scale) and in lattice units (upper scale).

condensate starts to decrease. These properties are in agreement with ChPT predictions (see Figs. 4 and 5 in paper [16]). An interesting prediction of ChPT is that in the whole region, where ChPT is applicable, a relation between the chiral condensate and the diquark condensate holds: $\langle qq\rangle^2 + \langle\bar{q}q\rangle^2 = \text{const}$ [14]. Note that this "circle relation" is valid only in the leading-order approximation, and it is violated by the next-to-leading-order corrections [17]. Our lattice results allow us to address the question of how well this relation is satisfied. In Fig. 7, we plot the combination $\sqrt{\langle qq\rangle^2 + \langle\bar{q}q\rangle^2}$ as a function of μ. From this plot, one sees that for the diquark source $\lambda = 0.001$ this relation is well satisfied up to $\mu < 263$ MeV ($\mu a < 0.15$). For bigger μ values, one can see the deviation from the circle relation for all values of the diquark source λ under consideration. Note also that for the values $\lambda = 0.00075$ and 0.0005, which move the system closer to the phase transition, the deviation from the circle relation is clearly seen in the transition region $\mu \in [176; 246]$ MeV ($\mu a \in [0.1; 0.14]$). The smaller the source λ that is chosen, the larger the deviation is. We believe that the deviation of our results from the relation $\sqrt{\langle qq\rangle^2 + \langle\bar{q}q\rangle^2} = \text{const}$ in the region $\mu \in [176; 246]$ MeV can be explained by the closeness of the system to the transition point, where a mean field study of ChPT is not applicable.

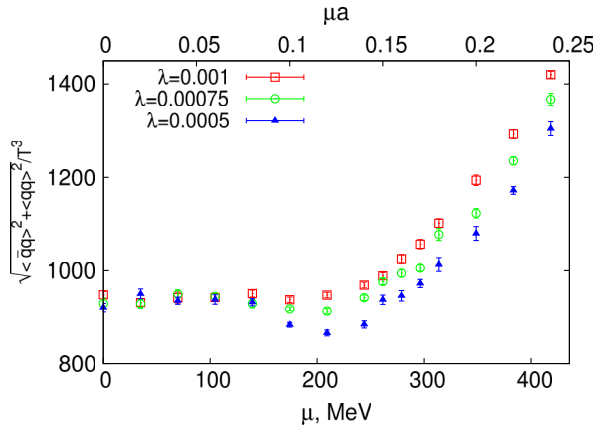

FIG. 7. The combination $\sqrt{\langle qq\rangle^2 + \langle\bar{q}q\rangle^2}/T^3$ of diquark and chiral condensates as a function of μ. The chemical potential is expressed in physical units (lower scale) and in lattice units (upper scale).

Now, let us consider the chiral condensate throughout the full region $\mu \in [0; 1759]$ MeV ($\mu a \in [0.0; 1.0]$). In Fig. 8, we plot the chiral condensate calculated for the smallest diquark source value $\lambda = 0.0005$ as a function of μ. It was noted above that the chiral condensate is practically insensitive to the values of λ, and thus the value of the chiral condensate at $\lambda = 0.0005$ can be taken as the value at $\lambda = 0$. According to ChPT, at $\mu > \mu^c$, the chiral condensate drops as

$$\langle\bar{q}q\rangle = \langle\bar{q}q\rangle_0 \left(\frac{\mu^c}{\mu}\right)^2, \tag{14}$$

where $\langle\bar{q}q\rangle_0$ denotes the chiral condensate at zero chemical potential. To check this prediction in the region $\mu \in [263; 352]$ MeV ($\mu a \in [0.15; 0.20]$), we fit our data by a power law $\langle\bar{q}q\rangle = A/\mu^\alpha$. This ansatz fits our data well ($\chi^2/\text{dof} = 0.3$) with the exponent $\alpha = 0.78(2)$. It is interesting to note that this fit gives a satisfactory description of the data up to $\mu \sim 1055$ MeV ($\mu a \sim 0.6$). Thus, one sees that the chiral condensate drops more slowly with increasing chemical potential than ChPT predicts. A similar slower decrease of the form $\langle\bar{q}q\rangle \sim 1/\mu$ was observed in Ref. [38] on the gauge ensembles generated with $N_f = 2$ Wilson quarks.

Good agreement with the leading-order ChPT prediction for the chiral condensate dependence on the chemical potential was found in Ref. [54] for $N_f = 1$ adjoint flavor and in Ref. [34] for $N_f = 4$ fundamental flavors, the latter

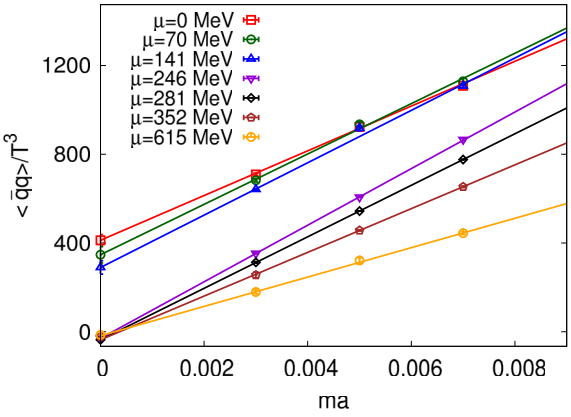

FIG. 9. The chiral limit of the chiral condensate $\langle\bar{q}q\rangle/T^3$, taken for different values of the chemical potential. The quark mass is expressed in lattice units.

study being carried out at $\beta = 1.5$. On the other hand, in Ref. [35], another lattice study at $\beta = 1.85$ was performed, where the chiral condensate was found to decrease as $\langle\bar{q}q\rangle \sim 1/\mu^{\alpha}$ with $\alpha = 1 \cdots 1.3$ depending on the λ value (see Table 3 of Ref. [35]). The same dependence of the $\langle\bar{q}q\rangle$ on the baryon chemical potential was also observed in Ref. [32] for $N_f = 8$ fundamental flavors at $\beta = 1.3$. We conjecture that the behavior of the chiral condensate is rather sensitive on the coupling regime of the theory. If β is small enough and the system is in the strong coupling regime, the leading order of ChPT is sufficient, and higher-order effects are weak.

Finally, it is interesting to study the chiral symmetry breaking in the chiral limit for different regions of the chemical potential. In Fig. 9, we plot the chiral condensate for different values of the chemical potential as function of the quark mass. As an example, we took a few values of the chemical potential in the hadronic phase, $\mu = 0$, 70, and 141 MeV ($\mu a = 0.0$, 0.04, 0.08, respectively); in the BEC phase, $\mu = 246$, 281, 352 MeV ($\mu a = 0.14$, 0.16, 0.20, respectively); and in the BCS phase, $\mu = 615$ MeV ($\mu a = 0.35$). At these fixed values of the chemical potential, we linearly extrapolated our data to $ma = 0$. It is seen from Fig. 9 that chiral symmetry breaking exists in the chiral limit within the hadronic phase (values $\mu = 0$, 70, and 141 MeV), whereas there is no chiral symmetry breaking in the chiral limit in the BCS phase ($\mu = 615$ MeV). We also found that the chiral limit of the chiral condensate at the points $\mu = 246$, 281, 352 MeV (in the BEC phase) are vanishing, but it is difficult to claim that there is no chiral symmetry breaking in the whole BEC phase; when we take the chiral limit, we change the pion mass and thus shift the critical point closer μ^c to zero. This effect is not important for the values of the chemical potential sufficiently far from the phase transition, but it might be important close to the phase transition. Note, that the absence of chiral symmetry breaking in the chiral limit within the BEC phase agrees with ChPT predictions.

C. Baryon density

In this section, we are going to consider the baryon number density n_B. It clear from formulas (5) and (9), that the baryon density depends on the square of the diquark source, λ^2, but not on λ. Thus, to get the baryonic density at zero diquark source, it is reasonable to fit our data for each value of the chemical potential by an ansatz, $n_B(\lambda) = A + B\lambda^2$.

In Fig. 10, we plot the baryon density in the region $\mu \in [0.0; 528]$ MeV ($\mu a \in [0.0; 0.3]$). It is clear that for all $\mu < 176$ MeV ($\mu a < 0.1$) the baryon density is vanishing within the uncertainty of the calculation. In the vicinity of the phase transition ($\mu \geq 176$ MeV), the baryon density starts to deviate from zero, and for larger values of the chemical potential, it rises with increasing μ. ChPT predicts that the dependence of the baryon density on the chemical potential above μ^c is given by a formula $n_B \sim \mu - \mu_c^4/\mu^3$. In the region $\mu \in [263; 352]$ MeV ($\mu a \in [0.15; 0.20]$), we fit our data by this formula in order to extract the critical chemical potential μ^c. The fit is of good quality, $\chi^2/\mathrm{dof} = 1.2$, and the result is $\mu^c = 207(7)$ MeV [$a\mu^c = 0.118(4)$]. This value is in agreement with our previous results for μ^c, obtained from the $\langle qq\rangle$ fits. From Fig. 10, it is visible that for bigger chemical potential, $\mu > 352$ MeV ($\mu a > 0.2$), our data deviate from the ChPT prediction.

Next, let us consider the baryon density at even larger values of the chemical potential. In Fig. 11, we plot the ratio n_B/n_0 as a function of μ, where for the square points the reference density n_0 is the baryon density for free continuum fermions at $T = 0$, $n_0 = (2\mu^3)/(3\pi^2)$ and for the circle points n_0 is the baryon number density for free lattice fermions. It can be seen that in the region $\mu \in [528; 1055]$ MeV ($\mu a \in [0.3; 0.6]$) these ratios are slowly varying functions of the chemical potential, taking values in the region 2.0…2.5, whereas the measured baryon density changes by an order of magnitude. We believe that the scaling of the baryon density $n_B \sim n_0$ confirms the

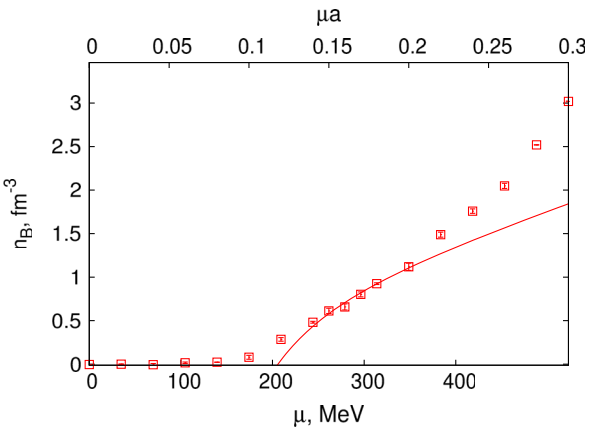

FIG. 10. The baryon density n_B in physical units, as a function of μ. The chemical potential is expressed in physical units (lower scale) and in lattice units (upper scale).

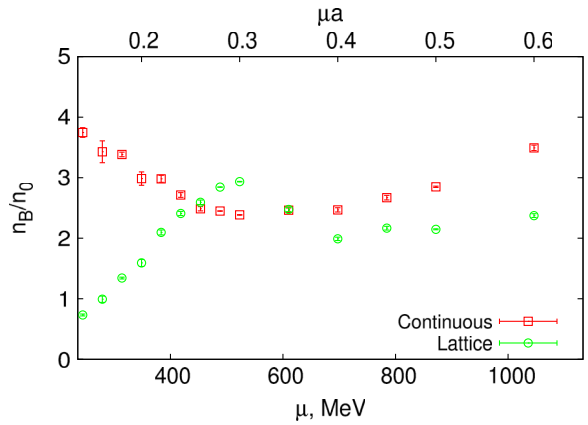

FIG. 11. The ratio n_B/n_0 as a function of the chemical potential μ. For the square points, the reference density n_0 denotes the baryon density for *free continuum fermions*, $n_0 = (2\mu^3)/(3\pi^2)$, whereas for the circle points the reference density n_0 denotes the baryon density for *free lattice fermions*. The chemical potential is expressed in physical units (lower scale) and in lattice units (upper scale).

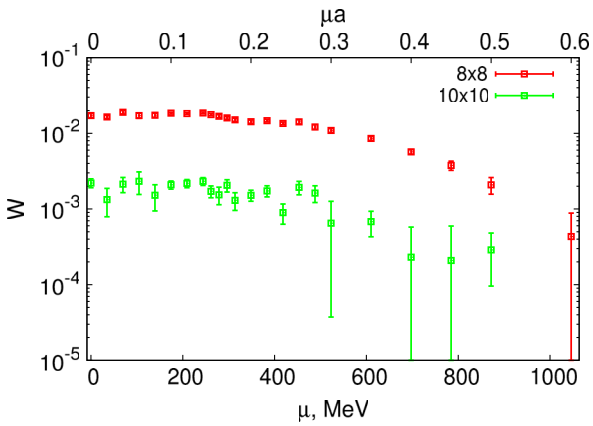

FIG. 12. The timelike Wilson loops for the contours 8×8 and 10×10 as a functions of the chemical potential μ.

conclusion that in the region $\mu \in [528; 1055]$ MeV the system is in a BCS-like phase. The relevant degrees of freedom in this phase are quarks, which mostly live inside the Fermi sphere with a condensate of Cooper pairs on the Fermi surface. At the same time, the fact that $n_B/n_0 \sim 2.0 \ldots 2.5$, but not ~ 1.0, can be attributed to UV and IR effects. Similar effects on the baryon density, although of smaller size ($n_B/n_0 \sim 1.1 \ldots 1.5$), were observed in Ref. [38] (see also the Fig. 6 therein for the demonstration of UV and IR artifacts in n_B).

D. Gluon observables

In this section, we study the gluon observables Polyakov loop (6) and Wilson loops (7). Similarly to the chiral condensate, the gluon observables are not sensitive to the value of the λ, and thus we take these observables calculated at the smallest value $\lambda = 0.0005$ as their values at the $\lambda = 0$.

We measured the average of the Polyakov loop as a function of the chemical potential. The result of this measurement is that for all values of the chemical potential studied in this paper the average Polyakov loop is vanishing within the uncertainty of the calculation.

Furthermore, in order to investigate the confinement properties of the system, we have calculated timelike Wilson loops (7) for the quadratic contours of the size 8×8 and 10×10 (for larger Wilson loops, we obtained results compatible with zero) as functions of the chemical potential. The same smearing strategy, as discussed in Sec. II.D, was employed for these Wilson loops measurements. The results are shown in Fig. 12. One learns from this plot that for $\mu > 352$ MeV ($\mu > 0.2$) the Wilson loops decrease with the growth of the chemical potential. At small μ, for $\mu \in [0; 263]$ MeV ($\mu a \in [0.0; 0.15]$), a plateau for both Wilson loops may be noticed. From these results, one can conclude that the system is in a confined phase for all values of the chemical potential under consideration. The possible explanation for this behavior may be the absence of the Debye screening in two-color QCD at zero temperature [18,55].

IV. DISCUSSION AND CONCLUSION

In conclusion, in this paper, we have carried out a low-temperature scan of the phase diagram of dense two-color QCD with $N_f = 2$ quarks. The study has been conducted using lattice simulations with rooted staggered quarks.

Our results can be summarized as follows. At small chemical potential $\mu < \mu^c = m_\pi/2 \sim 200$ MeV, we observe ahadronic phase. In this phase, QC_2D matter is in confinement, chiral symmetry is broken, the diquark condensate (10) vanishes, and the baryon number density is also zero. Relevant degrees of freedom in this phase are Goldstone bosons.

In the region $\mu^c < \mu < \mu^d \sim 352$ MeV, we observe the BEC phase. The characteristic feature of this phase is Bose-Einstein condensation of scalar diquarks. The order parameter for the transition to the BEC phase is the diquark condensate, which develops a nonzero value in the region $\mu > \mu^c$. Within the uncertainty of the calculation, $\mu_c = m_\pi/2$, where m_π is the pion mass at zero chemical potential. In this phase, QC_2D matter has also confining properties, whereas the baryon density is nonzero. Based on our detailed results for the onset of the diquark condensate, we believe that the transition from the hadronic to the BEC phase should be of the second order. Relevant degrees of freedom in the BEC phase are Goldstone bosons as well.

We have also found that the chiral limits of the chiral condensate at the points $\mu = 246$, 281, 352 MeV in the BEC phase are vanishing. Nevertheless, it is difficult to claim that there is no chiral symmetry breaking in the whole BEC phase, since when we take the chiral limit we change

the pion mass and thus shift the critical point μ^c. This effect is not important for the values of the chemical potential sufficiently far from the phase transition, but it might be essential close to the phase transition.

It is important to notice that for all values of the chemical potential $\mu < \mu^d$ our results are in good agreement with the predictions of ChPT. An exception is the chiral condensate, which drops with increasing chemical potential slower than ChPT predicts in leading order. This behavior of the chiral condensate might be explained by higher radiative corrections.

In the region $\mu > \mu^d$, our data start to deviate from ChPT predictions. The physical origin of this deviation can be understood as follows. At $\mu = \mu^d$, the baryon number density is $n_B \sim 1$ fm^{-3} (see Fig. 10). In SU(3) theory, a baryon density $n_B \sim 1$ fm^{-3} is of the order, when a gas of baryons cannot be considered as dilute anymore. The interactions of baryons at a density $n_B > 1$ fm^{-3} play an important role and cannot be taken into account as a perturbation, as it is done within ChPT. On the contrary, for a density $n_B < 1$ fm^{-3}, a gas of baryons can be considered as dilute, and ChPT is applicable. From this consideration, one may conclude that QC_2D in the region $\mu^c < \mu < \mu^d$ is an analog of the dilute baryon gas of SU(3) QCD. It is remarkable that the density at which one expects the transition from dilute gas to dense baryon matter in the SU(3) QCD is very close to that in the QC_2D.

If we further increase the chemical potential, starting from $\mu \sim 500 - 600$ MeV, one can observe that the diquark condensate scales as $\langle qq \rangle \propto \mu^2$ and the baryon density scales as $n_B \propto \mu^3$. Physically, this implies that the relevant degrees of freedom are quarks, which are mostly living inside the Fermi sphere with a condensate of Cooper pairs on the Fermi surface. These properties are clear hints in favor of the BCS phase. In this phase, the chiral symmetry is restored in the chiral limit. Our measurements of the timelike Wilson loops imply that the system still keeps the confinement property in this phase. In addition, our data confirm that the transition from the BEC to the BCS phase is smooth, if there is a phase transition at all.

The BCS phase extends up to $\mu \sim 1000$–1100 MeV. In the region $\mu \in [1100; 1410]$ MeV, the ratio $\langle qq \rangle / \mu^2$ drops, the baryon density scaling is $n_B \sim \mu^3$, the chiral condensate is very small, and the system is still retaining the confinement property. It is not quite clear what happens in this region, but most likely we are facing lattice artifacts, related with the fact that μa is close to 1. In the region $\mu > 1410$ MeV ($\mu a > 0.8$), the diquark condensate begins to drop, and n_B is close to saturation.

The results obtained in this paper are in reasonable agreement with the results of Refs. [33–35]. In these papers, the authors studied the phase diagram of QC_2D with $N_f = 4$ flavors of staggered fermions. What concerns a low-temperature scan of the phase diagram, these authors observed the succession of a hadronic phase and the BEC phase, with their properties well described by ChPT, but they did not find a BCS phase.

In Refs. [36–39], the QC_2D phase diagram with $N_f = 2$ flavors was studied through lattice simulation with Wilson fermions. In a low-temperature scan of the phase diagram, the authors observed a hadronic phase, followed by the BCS phase with deconfinement. Probably, the BEC phase has been missed in their simulations due to the violation of chiral symmetry by Wilson fermions. In addition, these authors observed the transition to the deconfinement phase at $\mu \sim 800$ MeV for a temperature $T = 47$ MeV [38]. In our study, we do not observe the transition to the deconfinement phase up to the chemical potential $\mu \sim 1410$ MeV. To understand the origin of the disagreement between our results and the results of the other groups, one should carry out more numerical simulations with different set of lattice parameters, but with the same N_f and at the same physical point.

It is interesting to mention the results of Ref. [6], where the phase diagram of SU(N_c) QCD was studied in the limit $N_c \to \infty$. The authors of this paper predicted the following phases: first, a hadronic phase is observed at sufficiently small chemical potential; when the chemical potential reaches $\mu = m_N/N_c$, the baryonic density ceases to vanish, and a phase of a dilute nuclear gas starts, which is similar to the BEC phase of the QC_2D theory. Further enhancing the chemical potential, this study has ended with the so-called "quarkyonic phase." In this phase, there is a Fermi sphere of quarks, at the surface of which baryons are living. The system is in confinement, but chiral symmetry is restored. We believe, that the quarkyonic phase at large N_c is similar to the BCS phase of the QC_2D theory.

Using this physical picture, it is not difficult to estimate the value of the chemical potential, where the quarkyonic phase becomes manifest. To do this, we note that the thickness of the surface layer, where strong interactions are important, is $\sim\Lambda_{\rm QCD}$. Then, the quarkyonic phase becomes manifest, when the volume inside the Fermi sphere $\sim 4/3\pi\mu^3$ becomes larger than the volume of the surface layer, modified by strong interactions, which is $\sim 4\mu^2\Lambda_{\rm QCD}$. Thus, we get $\mu > 3\Lambda_{\rm QCD}$. If we take $\Lambda \sim 200$ MeV, the quarkyonic phase starts at $\mu > 600$ MeV, which is in good agreement with the result of our present paper. One can also expect that the value of the chemical potential, where the quarkyonic phase starts in SU(3) theory is close to that in QC_2D, $\mu \sim 600$ MeV, since the $\Lambda_{\rm QCD}$ values in both theories are close to each other.

Finally, we summarize that in this paper we have carried out a low-temperature scan of the phase diagram for the QC_2D theory with two flavors of quarks. We have shown that the phase structure of this theory has a lot of similarities with SU(N_c) theory at large N_c. Since the predictions of the SU(N_c) theory at large N_c start to work already at $N_c = 2$, one can use QC_2D to make quantitative estimates for SU(3)

QCD with chemical potential, which is directly inaccessible due to the sign problem.

ACKNOWLEDGMENTS

Numerical simulations were performed at the supercomputer of Institute for Theoretical and Experimental Physics (ITEP), at the federal center for collective usage at National Research Center (NRC) "Kurchatov Institute" (http://computing.kiae.ru/) and at Moscow State University (MSU) supercomputer "Lomonosov". The work of A. Y. K. was supported by Russian Foundation for Basic Research (RFBR) Grant No. 16-32-00048 and Dynasty Foundation. The work of V. V. B., A. V. M. and A. A. N., which consisted of developing the program for generation of gluon configurations and studying the baryon density, chiral condensate and collecting statistics, was supported by the Russian Science Foundation (RSF) grant under Contract No. 15-12-20008.

[1] H.-T. Ding, F. Karsch, and S. Mukherjee, Thermodynamics of strong-interaction matter from Lattice QCD, Int. J. Mod. Phys. E **24**, 1530007 (2015).
[2] O. Philipsen, Proceedings, 29th John Hopkins Workshop on Current problems in particle theory: Strong matter in the heavens (JHW 2005), *Proc. Sci.*, LAT2005 (2006) 016; *Proc. Sci.*, JHW2005 (2006) 012.
[3] S. Muroya, A. Nakamura, C. Nonaka, and T. Takaishi, Lattice QCD at finite density: An Introductory review, Prog. Theor. Phys. **110**, 615 (2003).
[4] M. Buballa, NJL-model analysis of dense quark matter, Phys. Rep. **407**, 205 (2005).
[5] D. K. Hong, V. A. Miransky, I. A. Shovkovy, and L. C. R. Wijewardhana, Schwinger-Dyson approach to color superconductivity in dense QCD, Phys. Rev. D **61**, 056001 (2000); Erratum, Phys. Rev. D **62**, 059903(E) (2000).
[6] L. McLerran and R. D. Pisarski, Phases of dense quarks at large N_c, Nucl. Phys. **A796**, 83 (2007).
[7] M. Hanada and N. Yamamoto, Universality of phases in QCD and QCD-like theories, J. High Energy Phys. 02 (2012) 138.
[8] T. Gorda and P. Romatschke, Equation of state in two-, three-, and four-color QCD at nonzero temperature and density, Phys. Rev. D **92**, 014019 (2015).
[9] D. T. Son and M. A. Stephanov, QCD at Finite Isospin Density, Phys. Rev. Lett. **86**, 592 (2001).
[10] J. B. Kogut and D. K. Sinclair, Lattice QCD at finite isospin density at zero and finite temperature, Phys. Rev. D **66**, 034505 (2002).
[11] J. B. Kogut and D. K. Sinclair, Finite temperature transition for 2-flavor lattice QCD at finite isospin density, Phys. Rev. D **70**, 094501 (2004).
[12] P. de Forcrand, M. A. Stephanov, and U. Wenger, Proceedings, 25th International Symposium on Lattice field theory (Lattice 2007): Regensburg, Germany, July 30-August 4, 2007, *Proc. Sci.*, LAT2007 (2007) 237.
[13] G. Endrődi, Magnetic structure of isospin-asymmetric QCD matter in neutron stars, Phys. Rev. D **90**, 094501 (2014).
[14] J. B. Kogut, M. A. Stephanov, and D. Toublan, On two-color QCD with baryon chemical potential, Phys. Lett. B **464**, 183 (1999).
[15] K. Splittorff, D. T. Son, and M. A. Stephanov, QCD-like theories at finite baryon and isospin density, Phys. Rev. D **64**, 016003 (2001).
[16] J. B. Kogut, M. A. Stephanov, D. Toublan, J. J. M. Verbaarschot, and A. Zhitnitsky, QCD-like theories at finite baryon density, Nucl. Phys. **B582**, 477 (2000).
[17] K. Splittorff, D. Toublan, and J. J. M. Verbaarschot, QCD with two colors at finite baryon density at next-to-leading order, Nucl. Phys. **B620**, 290 (2002).
[18] T. Kanazawa, T. Wettig, and N. Yamamoto, Chiral Lagrangian and spectral sum rules for dense two-color QCD, J. High Energy Phys. 08 (2009) 003.
[19] C. Ratti and W. Weise, Thermodynamics of two-color QCD and the Nambu Jona-Lasinio model, Phys. Rev. D **70**, 054013 (2004).
[20] T. Brauner, K. Fukushima, and Y. Hidaka, Two-color quark matter: $U(1)_A$ restoration, superfluidity, and quarkyonic phase, Phys. Rev. D **80**, 074035 (2009); Erratum, Phys. Rev. D **81**, 119904(E) (2010).
[21] G.-f. Sun, L. He, and P. Zhuang, BEC-BCS crossover in the Nambu-Jona-Lasinio model of QCD, Phys. Rev. D **75**, 096004 (2007).
[22] L. He, Nambu–Jona-Lasinio model description of weakly interacting Bose condensate and BEC-BCS crossover in dense QCD-like theories, Phys. Rev. D **82**, 096003 (2010).
[23] N. Strodthoff, B.-J. Schaefer, and L. von Smekal, Quark-meson-diquark model for two-color QCD, Phys. Rev. D **85**, 074007 (2012).
[24] N. Strodthoff and L. von Smekal, Polyakov-quark–meson–diquark model for two-color QCD, Phys. Lett. B **731**, 350 (2014).
[25] L. von Smekal, Physics at all scales: The Renormalization Group. Proceedings, 49. Internationale Universitätswochen für Theoretische Physik, Winter School: Schladming, Austria, February 26-March 5, 2011, *Nucl. Phys. Proc. Suppl.* 228, 179 (2012).
[26] K. Kamikado, N. Strodthoff, L. von Smekal, and J. Wambach, Fluctuations in the quark-meson model for QCD with isospin chemical potential, Phys. Lett. B **718**, 1044 (2013).
[27] B. Vanderheyden and A. D. Jackson, Random matrix study of the phase structure of QCD with two colors, Phys. Rev. D **64**, 074016 (2001).

[28] T. Kanazawa, T. Wettig, and N. Yamamoto, Chiral random matrix theory for two-color QCD at high density, Phys. Rev. D **81**, 081701 (2010).
[29] T. Kanazawa, T. Wettig, and N. Yamamoto, Singular values of the Dirac operator in dense QCD-like theories, J. High Energy Phys. 12 (2011) 007.
[30] T. Kanazawa, T. Wettig, and N. Yamamoto, Banks-Casher-type relation for the BCS gap at high density, Eur. Phys. J. A **49**, 88 (2013).
[31] A. Nakamura, VII Warsaw Symposium on Elementary Particle Physics Kazimierz, Poland, May 21-25, 1984, Phys. Lett. **149B**, 391 (1984).
[32] S. Hands, J. B. Kogut, M.-P. Lombardo, and S. E. Morrison, Symmetries and spectrum of SU(2) lattice gauge theory at finite chemical potential, Nucl. Phys. **B558**, 327 (1999).
[33] J. B. Kogut, D. Toublan, and D. K. Sinclair, Diquark condensation at nonzero chemical potential and temperature, Phys. Lett. B **514**, 77 (2001).
[34] J. B. Kogut, D. K. Sinclair, S. J. Hands, and S. E. Morrison, Two-color QCD at nonzero quark-number density, Phys. Rev. D **64**, 094505 (2001).
[35] J. B. Kogut, D. Toublan, and D. K. Sinclair, The phase diagram of four flavor *SU(2)* lattice gauge theory at nonzero chemical potential and temperature, Nucl. Phys. **B642**, 181 (2002).
[36] S. Hands, S. Kim, and J.-I. Skullerud, Deconfinement in dense two-color QCD, Eur. Phys. J. C **48**, 193 (2006).
[37] S. Hands, S. Kim, and J.-I. Skullerud, Quarkyonic phase in dense two color matter, Phys. Rev. D **81**, 091502 (2010).
[38] S. Cotter, P. Giudice, S. Hands, and J.-I. Skullerud, Towards the phase diagram of dense two-color matter, Phys. Rev. D **87**, 034507 (2013).
[39] T. Boz, S. Cotter, L. Fister, D. Mehta, and J.-I. Skullerud, Phase transitions and gluodynamics in 2-colour matter at high density, Eur. Phys. J. A **49**, 87 (2013).
[40] I. Montvay and G. Münster, *Quantum Fields on a Lattice*, Cambridge Monographs on Mathematical Physics (Cambridge University Press, Cambridge, England, 1994).
[41] V. V. Braguta, A. Yu. Kotov, A. A. Nikolaev, and S. N. Valgushev, Pis'ma Zh. Eksp. Teor. Fiz. **101**, 827 (2015) [Lattice simulation study of SU(2) QCD with a nonzero baryon density, JETP Lett. **101**, 732 (2015)].
[42] Quark chemical potential is understood by μ here and below.
[43] P. Hasenfratz and F. Karsch, Chemical potential on the lattice, Phys. Lett. **125B**, 308 (1983).
[44] M. A. Clark, Proceedings, 24th International Symposium on Lattice Field Theory (Lattice 2006), *Proc. Sci.*, LAT2006 (2006) 004.
[45] M. A. Clark and A. D. Kennedy, Accelerating Dynamical-Fermion Computations Using the Rational Hybrid Monte Carlo Algorithm with Multiple Pseudofermion Fields, Phys. Rev. Lett. **98**, 051601 (2007).
[46] E. M. Ilgenfritz, M. Kalinowski, M. Müller-Preussker, B. Petersson, and A. Schreiber, Two-color QCD with staggered fermions at finite temperature under the influence of a magnetic field, Phys. Rev. D **85**, 114504 (2012).
[47] D. Scheffler, C. Schmidt, D. Smith, and L. von Smekal, Proceedings, 31st International Symposium on Lattice Field Theory (Lattice 2013), *Proc. Sci.*, LATTICE2013 (2014) 191.
[48] A. Hasenfratz and F. Knechtli, Flavor symmetry and the static potential with hypercubic blocking, Phys. Rev. D **64**, 034504 (2001).
[49] M. Albanese *et al.* (Ape Collaboration), Glueball masses and string tension in lattice QCD, Phys. Lett. B **192**, 163 (1987).
[50] V. G. Bornyakov, E. M. Ilgenfritz, and M. Müller-Preussker, Universality check of Abelian monopoles, Phys. Rev. D **72**, 054511 (2005).
[51] A. Bazavov *et al.*, Chiral and deconfinement aspects of the QCD transition, Phys. Rev. D **85**, 054503 (2012).
[52] Scale setting for $N_f = 4$ theory was performed in Ref. [46] on the lattice of the same size and with $ma = 0.01$, and the obtained Λ_L is nearly three times smaller than ours.
[53] Notice that one can use the other fitting functions to extrapolate our results to $\lambda = 0$. However, this will not change the main results of this paper.
[54] S. Hands, I. Montvay, S. Morrison, M. Oevers, L. Scorzato, and J. Skullerud, Numerical study of dense adjoint matter in two color QCD, Eur. Phys. J. C **17**, 285 (2000).
[55] D. H. Rischke, Debye screening and the Meissner effect in a two-flavor color superconductor, Phys. Rev. D **62**, 034007 (2000).